Desalination and Water Treatment
www.deswater.com
doi: 10.1080/19443994.2013.815690

52 (2014) 4721–4733
July

Taylor & Francis
Taylor & Francis Group

Preparation of some resorcinol formaldehyde resins for the separation of ^{134}CS from acidic waste streams

B. El-Gammal*, G.M. Ibrahim[1], I.M. El-Naggar

Hot Laboratories Center, Atomic Energy Authority, P.No. 13759, Cairo, Egypt
Email: belalelgammal@hotmail.com

Received 3 January 2012; Accepted 8 May 2013

ABSTRACT

An assortment of equilibrium assessments was conducted at 298 ± 2 K with a granulated resorcinol-formaldehyde (RF) resin, and acetone resorcinol formaldehyde gel (ARF) in an attempt to decontaminate ^{134}CS from waste streams. A: R: F: Na_2Co_3 was optimized as 2:1:2:1.6, during ARF preparation while, R: F: Na_2Co_3 was found to be 1: 3.5: 1.5 in case of RF, respectively. The obtained gels were amorphous and possessed different functional groups. The ARF had higher surface area and total pore volume values than RF; 780 m^2/g and 0.62 cm^3/g were the maximum values obtained for ARF under different conditions. The scanning electron microscope graphs proved that they are granular and spherical in nature with nanometer sizes under 22 W ultrasonic dispersion. In these tryouts, simulated waste sample to^{134}Cs was used in comparison with other radioactive ^{60}Co and $^{152+154}$. Lagergren first-order kinetic model was used to compare the kinetic constants, K_{ads} of the tested ions; the order of K_{ads} of $Cs^+ < Co^{2+} < Eu^{3+}$, which were in accordance with data obtained in the Cartesian coordinate in space. However, a reversed order of selectivity and capacity measurements was obtained because of hydration of the ions in solution.

Keywords: Resorcinol formaldehyde; Preparation; Characterization; Radioactive cesium; Decontamination; Waste streams

1. Introduction

Copious processes from nuclear facilities (fuel processing, power plants, laboratories, remediation or removal and others) initiate important volumes of radioactive liquid wastes, which should be treated in order to minimize their impact on environment [1–5]. Among those, radioactive cesium isotopes are ones of the most lavish fission products of uranium, which are dangerous to health. Gamma-emitter ^{134}Cs and ^{137}Cs with a half-life of 2 and 30 years, respectively, are mainly present in these fission products. Both isotopes are radiotoxic, because they are an analog of potassium and thus may be quickly assimilated into the body. They accumulate in the food chain and persist in the environment for hundreds of years. For these reasons, the problem of selective cesium effluent's decontamination has attracted a great deal of attention in recent years [6–9].

However, the use of classical inorganic sorbents such as manganese oxide, zeolites, iron hydroxide or

*Corresponding author.

[1]Current address: King Khaled University, Bisha Branch KSA.

barium sulfate usually employed for the extraction of various radioactive elements such as Sr, Co, Ni, or actinides is inefficient in the case of cesium due to their low affinity [8–10].

Thus, the elaboration of innovative materials able to remove radioactive cesium with a continuous process (such as a column process) and minimize the waste volume, matching with the classical waste confinement matrix, such as cement or glass, is a challenge for the cleanup of the contaminated sites [10–12].

Organic ion-exchange resins, such as the resorcinol-formaldehyde (RF), Duolite CS-100, Diphonix-CS, and SuperLig-644, have been used for cesium removal from Hanford Site nuclear waste solutions. Duolite CS-100, a polymer of phenol-carboxylic, is similar to the RF resin, but the resin was less selective for cesium over sodium, and multiple loading and elution cycles. Therefore, the development of RF characteristics is necessary [13].

In this work, RF and acetone resorcinol formaldehyde (ARF) gels were prepared under various conditions of catalyst, surfactant, ultrasonic dispersion, and different drying conditions to obtain controlled morphology, surface area, porosity and internal coordinates, with high selectivity towards simulated or active ^{134}Cs.

2. Experimental

2.1. Preparation of RF and ARF carbon gels

In this work, the entire chemicals used were research grade, except for formaldehyde. According to scheme preparation of RF, graphically represented in Fig. 1, RF carbon gels were synthesized via the sol–gel polycondensation of resorcinol (1,3-dihydroxybenzene) ($C_6H_4(OH)_2$) (R) and formaldehyde (HCHO) (F) in a slightly basic aqueous solution to give 2,4-bis (hydroxymethyl)benzene-1,3-diol.

Sodium hydroxide and/or sodium carbonates were used as a separate catalyst alkaline media, while double-distilled water was used as both solvent and diluent, and 2,4-bis(hydroxymethyl)benzene-1,3-diol is deprotonated by the action of heat to (2,6-dihydroxy-3-(hydroxymethyl)phenyl)methylium, which both recombine together to 4-(2,6-dihydroxy-3-(hydroxymethyl)benzyl)-2,6-bis(hydroxymethyl)benzene-1,3-diol and finally to RF resins.

The optimized molar ratios of resorcinol: formaldehyde: alkaline solution was 1: 3.5: 1.5, where, 37% formaldehyde as commercial aldehyde solution was selected, and the alkaline solution was used to dissolve the resorcinol solid.

As shown in Fig. 2, acetone and formaldehyde were converted into 1, 5-dihydroxypentan-3-one by the action of alcoholic KOH solution. In presence of Na_2CO_3, 1, 5-dihydroxypentan-3-one can react directly with resorcinol to form ARF resin. The optimized molar ratio A: R: F: Alk. solution was found to be 2:1:2:1.6, respectively.

The RF and ARF mixtures were suspended in a vegetable palm oil, magnetically stirred and dispersed by ultrasonic irradiation in the range 0–200 W; 22 W was found to be an optimized one.

Gelation temperature was 308 K. The sample size is 4 cm in length and 3 mm in diameter. Before drying process, RF gels were solvent-exchanged with t-butanol for three times. RF gels were dried by freeze-drying at 263 K for 3 h [3,6] and microwave drying (200 W microwave oven Eurotherm (model TRX—2021) at one atmosphere with 10 min drying time). Pyrolysis temperature was 1,023 K under nitrogen flow (200 cm^3/min).

2.2. Characterization of the produced gels

Elemental analysis of ARF and RF resins was achieved using CHNSO flash analyzer, Model EA 1100 Series, Finnigan Company, USA.

Bruker DRX, 500 MHz Spectrometer, BRUKER Bio-Spin Group, USA, collected the 1HNMR and 13CNMR spectra of the resins using solid-state NMR spectroscopy technique.

The porous properties of RF and ARF gels were determined by the N_2 adsorption method using an adsorption apparatus (Nova3000 series, USA). BET surface area (SBET), mesopore size distribution, and mesopore volume (V_{mes}) were evaluated. The nitrogen adsorption/desorption isotherms were measured at 77 K and at the relative partial pressure (i.e. P/P0) of N_2 of 0.98, after degassing the samples at 100 °C for 5 h.

The distinctive porosities of the different ARF and RF resins were measured by mercury intrusion porosimetery (MIP), using Micromeritics 9,320 Pore Size Analyzer.

The cross-sections of RF and ARF carbon gels were observed by a scanning electron microscope (SEM) (JEOL, JSM-6700F).

Synchronized thermal analysis, DTA and thermogravimetric procedure, TG was carried out in order to study the thermolysis of the hybrid materials using a Shimadzu simultaneous DTA-TG50 analyzer, Shimadzu, Japan.

The phase evolution at various stages of synthesis was analyzed using Shimadzu X-ray diffractometer, Model XD 490, Japan) with Cu–Kα radiation and Bragg–Brentano focusing geometry was employed.

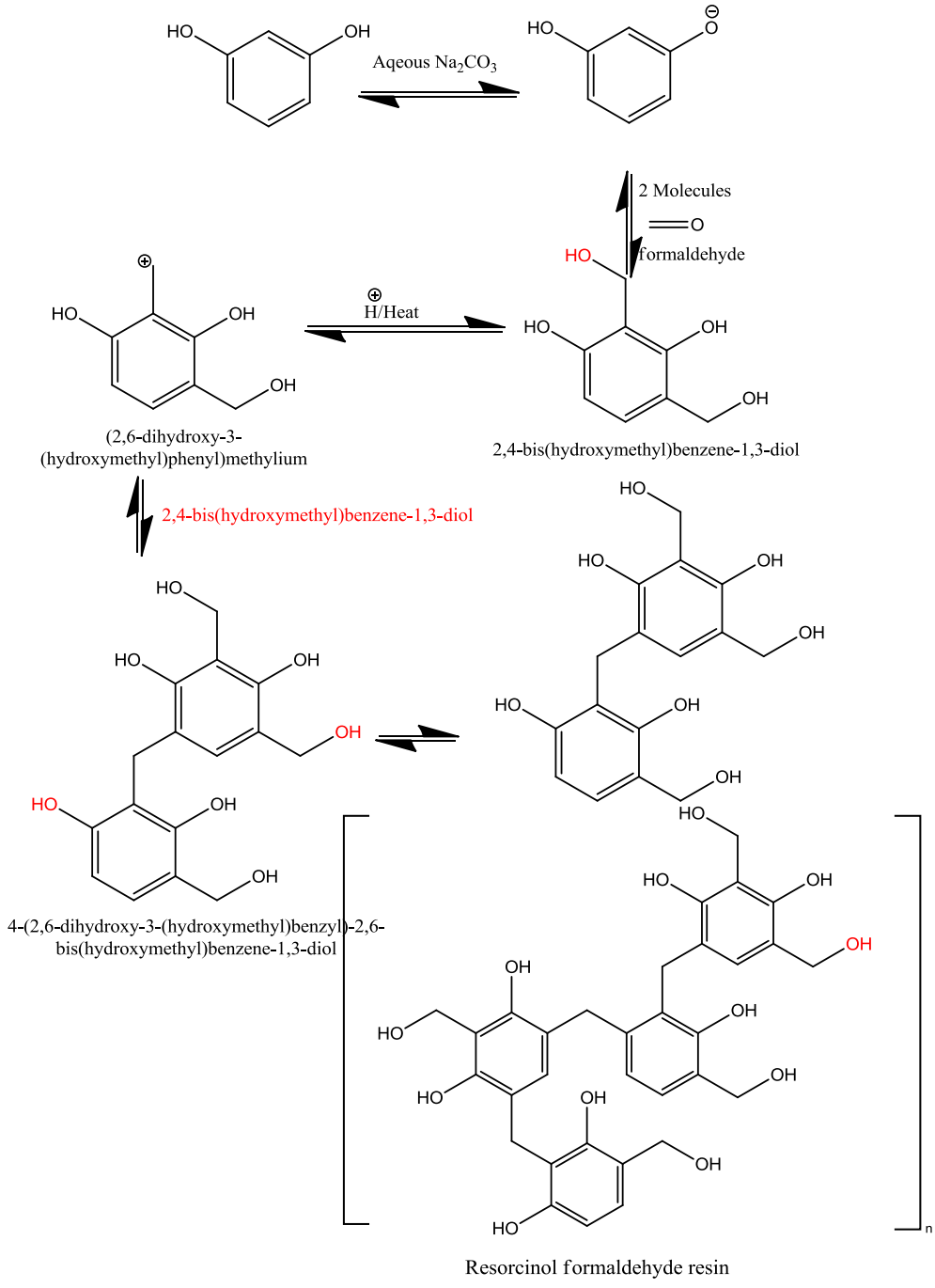

Fig. 1. Preparation scheme for RF resin using Na_2CO_3 as a catalyst.

Fourier transforms infrared (FTIR), spectrophotometer BOMEM FTIR Model 157, Canada was used 400–4,000 cm^{-1} for studying the spectra of the prepared hybrid materials.

2.3. Sorption investigations

Cs^+ sorption experiments on both ARF and the RF were performed; firstly, by using nonradioactive Cs^+ containing aqueous solutions in order to investigate the sorption kinetics. Sorption isotherms were plotted from data obtained at reaction equilibrium. So that equilibrium studies in sterile water were performed before isotherm sorption experiments also in pure water. All Cs^+ extraction experiments were performed in batch solution under shaking at room temperature.

For the equilibrium studies, 10 mg of the ARF and RF was shaken in 20 mL of a 10^{-2} M of $CsNO_3$

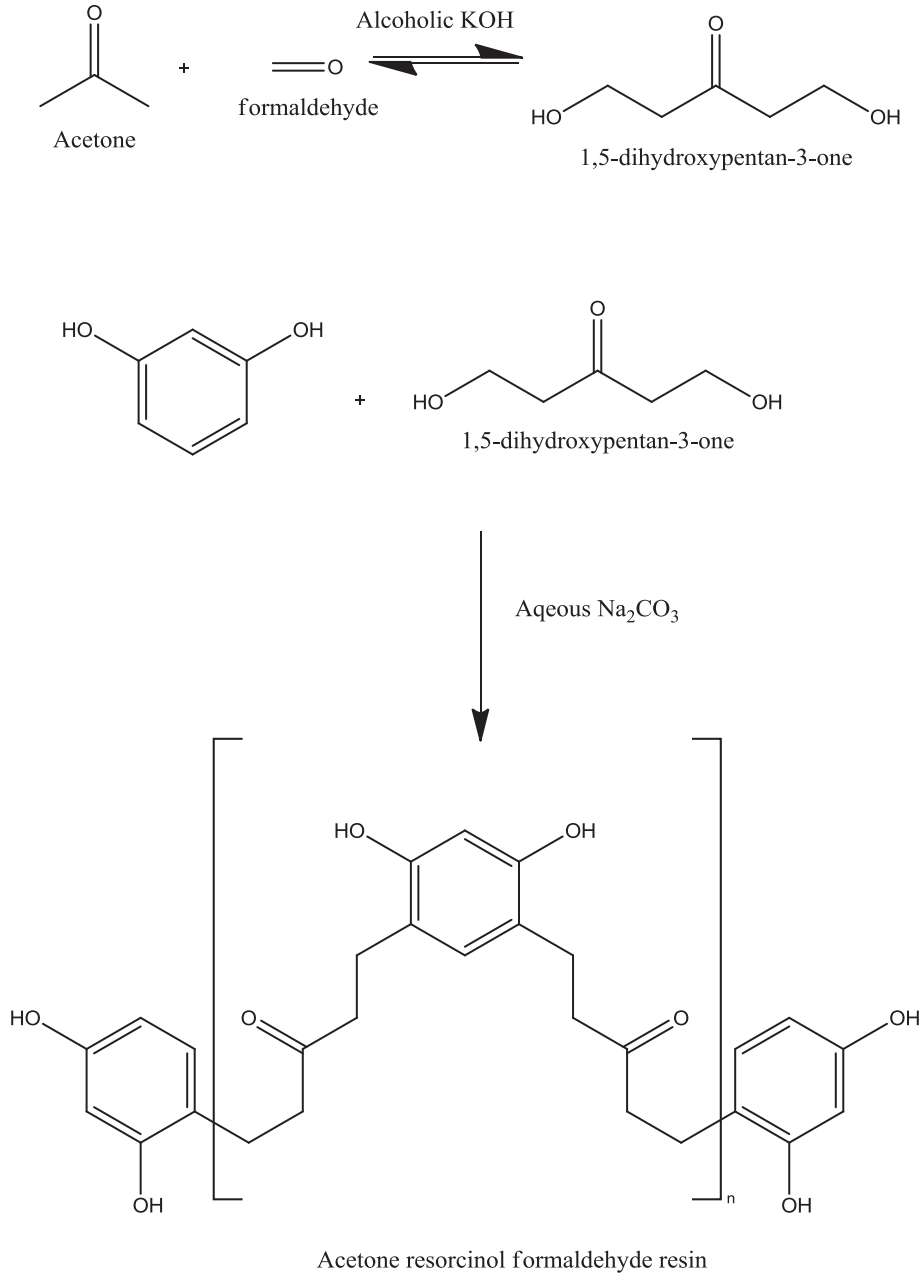

Fig. 2. Preparation scheme for ARF resin using Na_2CO_3 as a catalyst.

solution in deionized water. Experiments were performed from five min to two days. Then, the nanocomposite was separated from the liquid phase by filtration through a 0.2 mm cellulose acetate membrane and the remaining Cs^+ concentration of the supernatant was measured using ionic chromatography. To determine the time required to reach equilibrium, the time dependence of the adsorbed cesium quantity, Q_t, (mmol/g) was used and is defined as follows:

$$Q_t = (C_0 - C_t)\frac{V}{m} \quad (1)$$

where C_0 (mmol/L) is the initial concentration of cesium, C_t (mmol/L) is the remaining concentration of cesium in solution after the specified time t (min), V (L) is the volume of the solution, and m (g) is the mass of adsorbent.

First-order kinetics is expressed as the solute removal rate that controls the residence time of the

sorbate in the solid/solution interface. Lagergren and Svenska derived the pseudo-first-order rate expression based on solid capacity, q, which is generally expressed as follows [9]:

$$\frac{dq}{dt} = k_{ads}(q_e - q) \quad (2)$$

Integration of Eq. (4) with the boundary conditions as follows: at $t = 0$, $q = 0$, and at $t = t$, $q = q_t$, gives:

$$\log(q_e - q_t) = \log q_e - \left(\frac{k_{ads}}{2.303}\right)t \quad (3)$$

Eq. (5) can be written in its non-linear form as:

$$q_t = q_e(1 - \exp(-k_{ads}t)) \quad (4)$$

where q_e and q_t are the amounts of the metal ions adsorbed (mmol g^{-1}) at equilibrium and at time t (h), respectively, and k_{ads} is the sorption rate constant (time^{-1}). Hypothetically, to ascertain the rate constants and equilibrium metal ion uptake, the straight-line plots of log ($q_e - q_t$) against t of Eq. (5) should be constructed; the rate constants (k_{ads}) and theoretical equilibrium sorption capacities, q_e (theo.), can be calculated from the slopes and intercepts.

For capacity studies, a first parent solution of 1 M of Cs^+ was prepared by dissolving $CsNO_3$ in deionized water. Solutions with Cs^+ concentrations ranging from 0.0001 M to 0.01 M were prepared by diluting the parent solution with deionized water. In each experiment, 10 mg of sorbent nanocomposite were added to 20 mL of investigated solutions for 24 h, the time at which the equilibrium is always reached. Then, the ARF and RF gels were separated from the liquid phase by filtration through a 0.2 mm cellulose acetate membrane. The remaining Cs^+ concentration of the liquid phase was then analyzed by atomic absorption spectrometry. To establish the adsorption isotherm, the remaining solute concentration of the cesium at equilibrium, C_e, (mmol/L) was compared with the quantity of the cesium retained on solid particles (ARF and RF gels or bulk materials), Q_e, (mmol/g). The cesium concentration retained in the solid particles at equilibrium is given by the equation [11]:

$$Q_e = (C_0 - C_e)\frac{V}{m} \quad (5)$$

where V is the volume of solution (L), m is the mass of the sorbent (ARF or RF) used (g), C_0 is the initial concentration of cesium in solution (mmol/L) and C_e is the equilibrium concentration of the cesium in solution (mmol/L).

Batch technique was followed to study the distribution coefficient, K_ds of Cs^+, Co^{2+} and Eu^{3+} ions on ARF and RF at constant pH = 4. Where 0.05 g of the exchanger was shaken at 25 ± 1°C with 5 mL metal nitrate solutions at a V/m ratio of 100 ml g^{-1} of 10^{-4} M of the ions labeled with radioactive ^{134}Cs, ^{60}Co and $^{152+154}Eu$, respectively. After an overnight standing, the mixtures were centrifuged and the pH of the solution was determined using pH meter, model 601 A, USA. The K_d values were calculated according to the following equation [11]:

$$K_d = \frac{(A_0 - A)}{A} \times \frac{V}{m} \quad (6)$$

where A_o and A are the initial and final activity of the radioactive isotope. For radiometric assay, cesium, cobalt, and/or europium nitrates solutions labeled with ^{134}Cs, ^{60}Co, and $^{152+154}Eu$ on a shaker thermostat adjusted at 298 ± 1 K and attained for equilibrium were identified and measured by gamma-ray spectrometry using a TENNELEC Multichannel analyzer coupled with a high-purity Germanium detector with measuring error not exceeding ± 3%.

3. Results and discussion

3.1. Surface area and porosity

Surface area and porosities of the different gels were conducted in two parallel techniques, namely,

Table 1
Preparation conditions and surface features of RF and ARF resins using 1:3.2:1.3 and 1:3.5:1.5 molar ratios, respectively

Reactant ratios	Ultrasonic irradiation	Drying method	V_{mes} (cm^3/g) ± 0.04–0.076	S_{BET} (m^2/g) ± 0.03–0.89
RF (R:F:Alk. Solution)				
1:3:1	√	Microwave	0.89	615
2:1:2	√	Microwave	0.91	530
1:3.2:1.3	√	Freeze	0.63	722
1:3.1:1.1		Microwave	0.59	653
1:3.5:1.5	√	Freeze	0.62	733
2:1:2		Microwave	0.43	518
RF (A:R:F:Alk. Solution)				
2:1:2:1.6		Microwave	0.45	732
2:1:2:1.6	√	Microwave	0.45	780
2:1:2:1.6	√	Freeze	0.62	728
1:1:2:1		Microwave	0.29	615
1:1:2:1	√	Freeze	0.12	348
1:1:2:1	√	Microwave	0.19	653

BET-method and MIP technique. The synthesis conditions and porous properties of carbon gels prepared by ultrasonic irradiation during the gelation process and various drying methods are shown in Table 1.

The freeze-dried and microwave-dried RF and ARF gels pore size distributions are independent of the surface area measurements. The mesoporous volumes obtained were highest at 2:1:2 molar ratio of R: F: Alk. Solutions and recorded 0.91 ± 0.04 mL/g upon microwave drying process. As it could be seen in Table 1, the ultrasonic dispersion had no effect on the obtained mesopore volumes. In case of ARF gels, the ultrasonic dispersion had no effect on the V_{mes}, except for on using A: R: F: Alk. Solution molar ratio of 1: 1: 2: 1. [14].

However, S_{BET} values were affected by the molar ratio, drying process, and/or the ultrasonic dispersion. Generally, the ultrasonic irradiation would raise the S_{BET} values. In case of RF gels, 722 and 733 m^2/g were obtained for 1: 3.2: 1.3 and 1: 3.5: 1.5 molar ratios, respectively. This could be assigned to the decreased particle size obtained upon ultrasonic dispersion procedure as demonstrated by the SEM nanographs in Fig. 3.

3.2. Morphological aspects

As it could be seen in Fig. 3, the particle size of the emulsified ARF and RF is slightly larger than that of the dried gels; the particle size of the emulsified ARF and RF gels is about 100 nm with blue-grey and pink colors, respectively. Upon freeze-drying, the gels shrink to lower particle's sizes, with fissures and cracks in the gel spheres due to rapid withdrawal of the solvent from the inner structure of the gels. The particle diameters of the ARF resins are about 50–70 nm, while that of the RF gels are in the same range, but with non-uniform structures [15].

3.3. FTIR spectroscopy

The infrared studies of R–F and ARF revealed that two distinct peaks at 760 and 820 cm^{-1}, respectively,

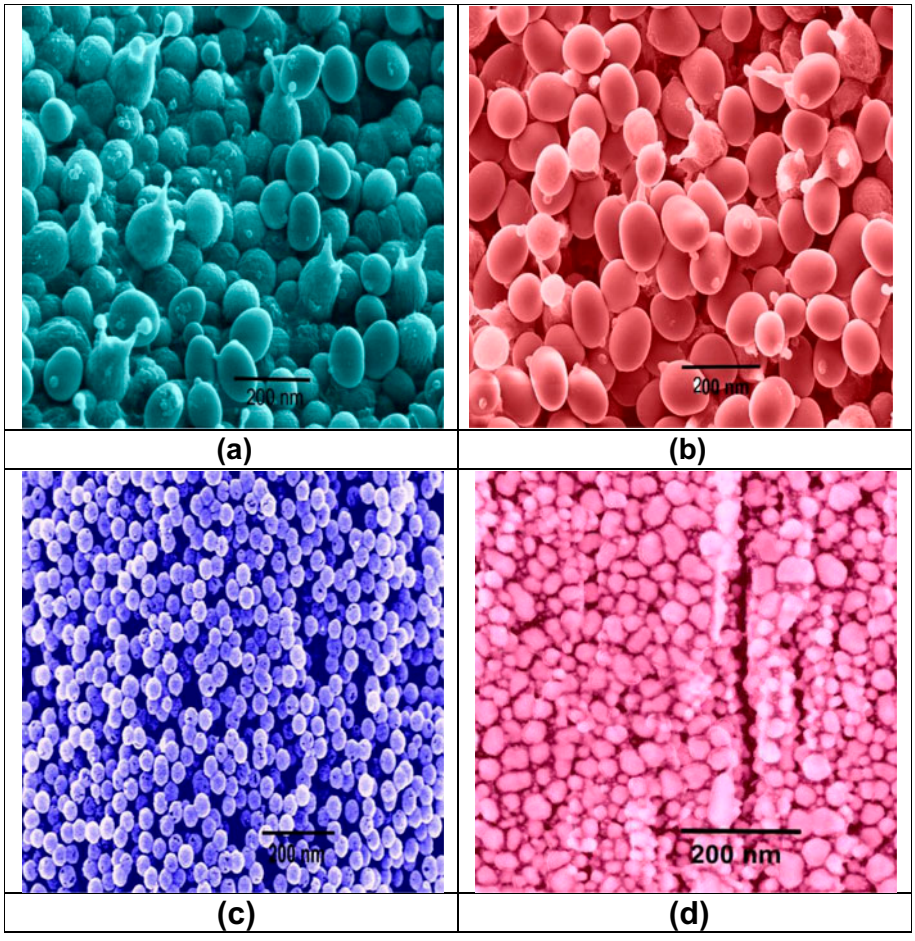

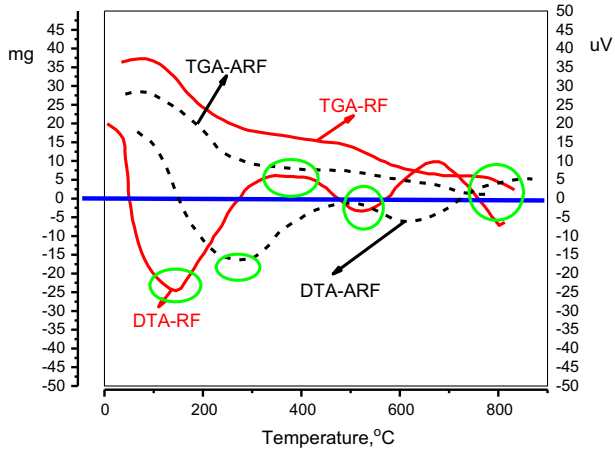

Fig. 3. Thermal behavior of ARF and RF gels.

due to the presence of aromatic rings in both moieties. Broad bands at about 2,780–3,500 cm^{-1} are assigned to symmetrical and anti-symmetrical stretching vibrations of water molecules with hydrogen bonding. The bands that exist at 1,640 and 1,650 cm^{-1} are due to presence of free water molecules. Two bending bands at about 1,450 and 1,500 cm^{-1}, respectively, indicate the phenolic hydroxyl groups. The stretching of the C–O group appears at 1,050 and 1,100 cm^{-1}. In case of ARF, a single strong band at about 1,715 cm^{-1} appeared due to presence of ketonic C=O [16].

3.4. XRD and thermal studies

The diffraction patterns of both ARF and RF revealed that these structures were amorphous in nature and there was no improvement of crystallinity under heat treatment, as they may decompose at slightly higher temperatures as revealed by the thermogravimetric studies, as shown in Fig. 3. The free water began to escape from the RF and ARF structures at about 88 and 100°C, respectively, giving rise 12 and 13% loss of water, respectively and corresponds to endothermic behaviors at the same temperatures. The second weight losses of both compounds were in the range between 400°C and 670°C, corresponding to exothermic behaviors between these temperatures, which is attributed to decomposition and burning of prepared carbon gels [17].

Figs. 4–9 show the ^{1}HNMR spectra and ^{13}CNMR of the basic resorcinol, RF and ARF. The spectra show that resorcinol, formaldehyde, and acetone were consumed throughout preparation, by the help of KOH as a basic medium and a catalyst at the same time. The ^{1}HNMR of resorcinol is shown in Fig. 4. Two singlets were observed at s-5.35 ppm and s-6.27 ppm

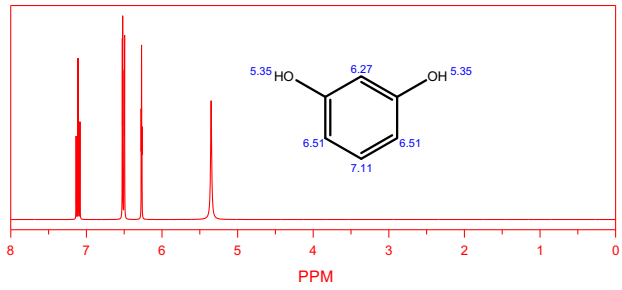

Fig. 4. Resorcinol ^{1}H NMR spectra.

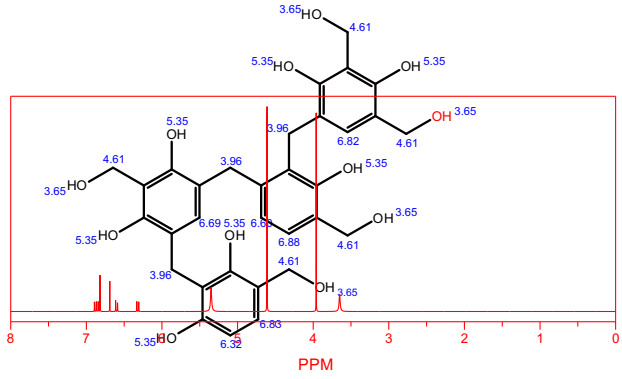

Fig. 5. RF ^{1}H NMR spectra.

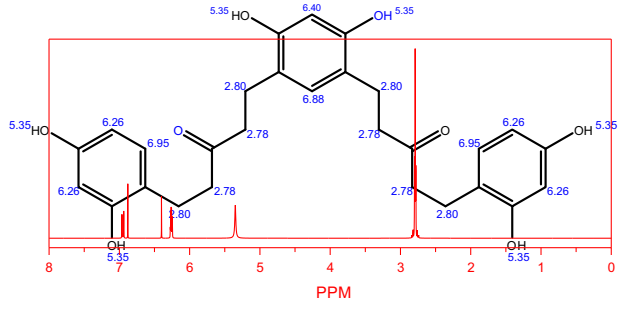

Fig. 6. ARF ^{1}H NMR spectra.

due to the presence of the phenolic OH groups and the adjacent CH between these phenolic groups, individually. On the other hand, two triplets could be attributed to the remaining aromatic CH groups at 6.51 and 7.11 ppm [18].

Due to the formation of ARF and RF resins, the ^{1}HNMR triplets of resorcinol absolutely disappeared and converted into singlets as shown in Fig. 5. However, the ^{1}HNMR of ARF resins shown in Fig. 6 showed multiplet peaks at t−2.7 and t−6.95 ppm due to the formation of aliphatic CH groups and shift to higher shielding values [18].

Figs. 7–9 show the ^{13}CNMR spectra of R, RF, and ARF and their predicted chemical shifts on the vertices of the assigned structures. Before its reaction with formaldehyde, or acetone and formaldehyde, resorcinol possessed 4 peaks at different positions. The sharpest one is assigned to the two C–OH groups of the phenolic ring at about δ 159 ppm. Nearly, the same intensity was observed for the two symmetrical ortho-CH groups at about δ 108 ppm. The OHC–C*–COH of the benzene ring showed an intermediate peak at about δ 103 ppm, while the sixth carbon atom of the resorcinol had a peak at about δ 131 pp. upon reaction with formaldehyde in case of RF, or with acetone and formaldehyde in case of ARF, these peaks are relocated to lower δ, due to the formation of new compounds. Different peaks were observed in the δ 20–60 ppm, which are assigned to the aliphatic carbons in RF and ARF. In addition, distinct bands were detected at δ 210 ppm, which reveal the presence of carbonyl groups on the ARF resin [18].

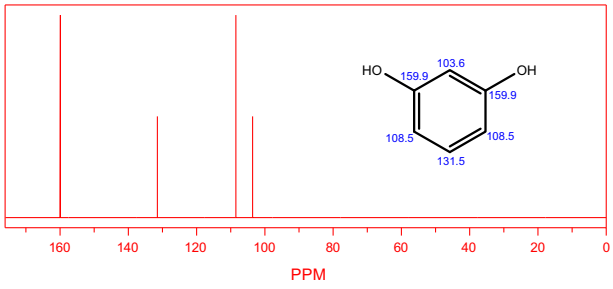

Fig. 7. Resorcinol ^{13}CNMR spectra.

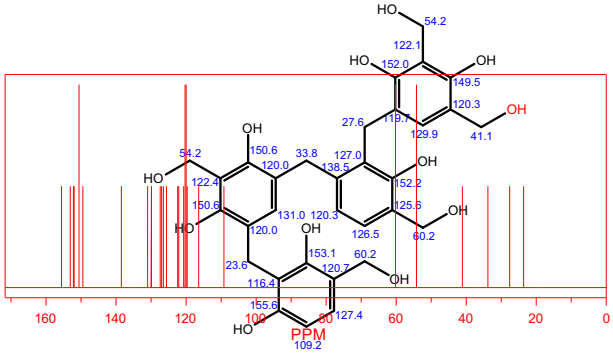

Fig. 8. RF ^{13}CNMR spectra.

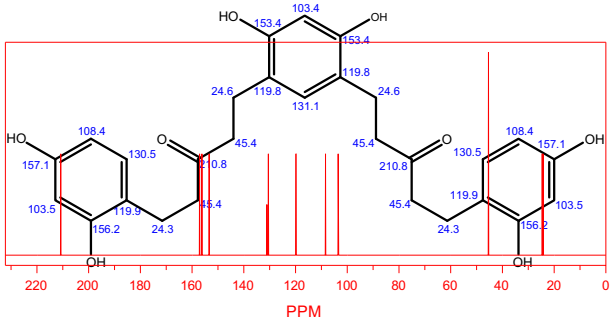

Fig. 9. ARF ^{13}CNMR spectra.

3.4.1. Spatial and sorption relationships

Figs. 10 and 11 represent a good simulation of the prepared ARF and RF gels in space, as a consequence of their structure prediction with the data obtained by proton magnetic resonance and carbon magnetic resonance spectroscopy. During the sorption process of cesium, cobalt, and/or europium nitrates solutions labeled with ^{134}Cs, ^{60}Co, and $^{152+154}$Eu on ARF and RF resins. These ions should diffuse from the bulk solution to the bulk gels, which would depend upon the internal structure of the gels. Tables 2 and 3 describe the detailed structures of Figs. 10 and 11 in space, using both Cartesian coordinates x, y, and z, as well as the internal coordinates as a function of the atom positions, their bond lengths and the angles between these bonds. Despite the amorphous nature of ARF and RF gels, their structures are in accordance with the stretching and bending data obtained by the FTIR spectroscopy [17,19].

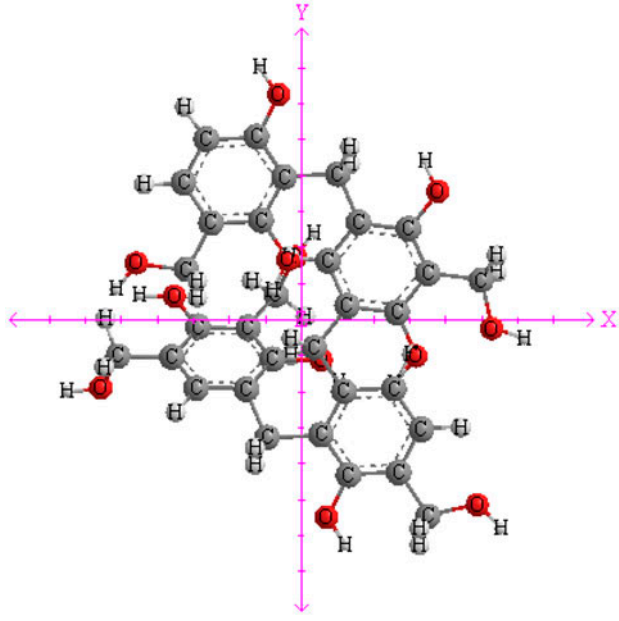

Fig. 10. Spatial configuration of RF resin in 3D-coordinates.

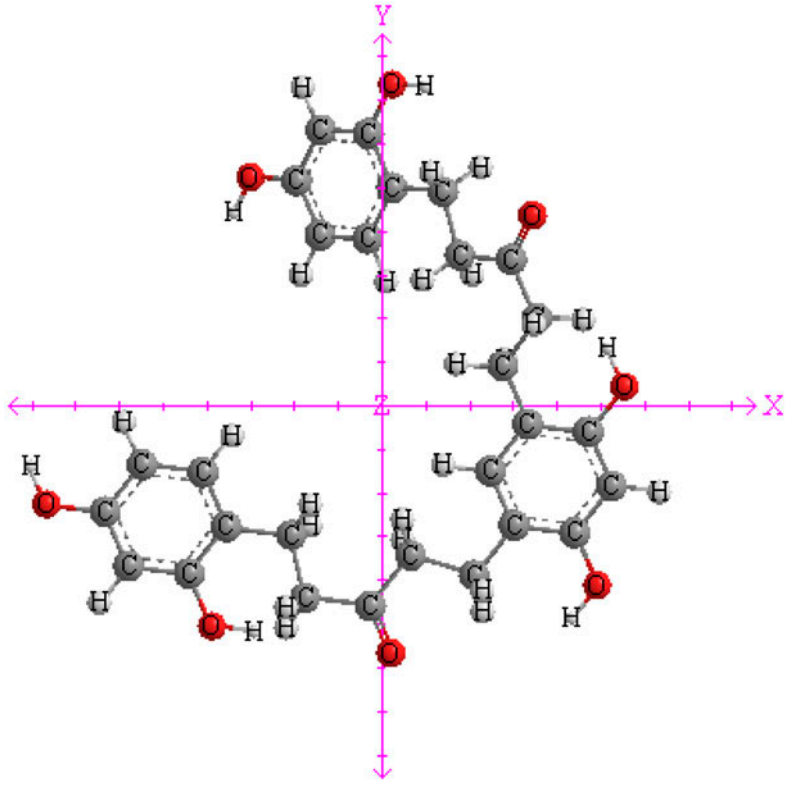

Fig. 11. Spatial configuration of ARF resin in 3D-coordinates.

Table 2
Spatial coordinates, Cartesian coordinates, internal coordinates and their corresponding angles of ARF gel

Cartesian coordinates				Internal coordinates							
Atom	X (Å)	Y (Å)	Z (Å)	Atom	Bond atom	Length Ao	Angle atom	Angle (o)	2nd angle atom	2nd angle (o)	
O(1)	4.92	5.42	0.00	C(2)							
C(2)	6.10	4.74	0.00	C(3)	C(2)	1.34					
C(3)	7.26	5.41	0.00	O(1)	C(2)	1.36	C(3)	120.00			
C(4)	8.41	4.74	0.00	C(8)	C(2)	1.34	O(1)	120.00	C(3)	120.00	Pro-R
O(5)	9.59	5.42	0.00	C(4)	C(3)	1.34	C(2)	120.00	O(1)	−180.00	Dihedral
C(6)	8.41	3.41	0.00	H(38)	C(3)	1.10	C(2)	120.00	C(4)	120.00	Pro-S
C(7)	7.26	2.74	0.00	O(5)	C(4)	1.36	C(3)	120.00	C(2)	180.00	Dihedral
C(8)	6.10	3.41	0.00	C(6)	C(4)	1.34	C(3)	120.00	O(5)	120.00	Pro-S
C(9)	10.74	−1.10	0.00	C(7)	C(8)	1.34	C(2)	120.00	O(1)	180.00	Dihedral
C(10)	10.74	0.41	0.00	C(14)	C(6)	1.50	C(4)	120.00	C(7)	120.00	Pro-R
O(11)	11.79	1.01	0.00	C(19)	C(8)	1.50	C(2)	120.00	C(7)	120.00	Pro-S
C(12)	9.43	1.16	0.00	H(40)	C(7)	1.10	C(6)	120.00	C(8)	120.00	Pro-R
C(13)	9.30	−1.61	0.00	C(12)	C(14)	1.52	C(6)	109.50	C(4)	−180.00	Dihedral
C(14)	9.71	2.66	0.00	H(47)	C(14)	1.11	C(6)	109.44	C(12)	109.44	Pro-S

(*Continued*)

Table 2 (*Continued*)

Cartesian coordinates				Internal coordinates							
Atom	*X* (Å)	*Y* (Å)	*Z* (Å)	Atom	Bond atom	Length Ao	Angle atom	Angle (o)	2nd angle atom	2nd angle (o)	
C(15)	3.64	3.65	0.00	H(48)	C(14)	1.11	C(6)	109.46	C(12)	109.46	Pro-R
C(16)	2.34	2.89	0.00	C(10)	C(12)	1.51	C(14)	109.50	C(6)	180.00	Dihedral
O(17)	1.29	3.50	0.00	H(43)	C(12)	1.11	C(10)	109.44	C(14)	109.44	Pro-R
C(18)	2.34	1.38	0.00	H(44)	C(12)	1.11	C(10)	109.46	C(14)	109.46	Pro-S
C(19)	4.80	2.66	0.00	C(9)	C(10)	1.51	C(12)	120.00	C(14)	180.00	Dihedral
C(20)	0.90	0.87	0.00	O(11)	C(10)	1.21	C(9)	120.00	C(12)	120.00	Pro-R
O(21)	11.64	−3.10	0.00	C(13)	C(9)	1.52	C(10)	109.50	O(11)	−180.00	Dihedral
C(22)	10.46	−3.78	0.00	H(41)	C(9)	1.11	C(10)	109.44	C(13)	109.44	Pro-S
C(23)	10.46	−5.11	0.00	H(42)	C(9)	1.11	C(10)	109.46	C(13)	109.46	Pro-R
C(24)	9.30	−5.78	0.00	C(28)	C(13)	1.50	C(9)	109.50	C(10)	−180.00	Dihedral
O(25)	9.30	−7.14	0.00	H(45)	C(13)	1.11	C(9)	109.44	C(28)	109.44	Pro-S
C(26)	8.15	−5.11	0.00	H(46)	C(13)	1.11	C(9)	109.46	C(28)	109.46	Pro-R
C(27)	8.15	−3.78	0.00	C(22)	C(28)	1.34	C(13)	120.00	C(9)	0.00	Dihedral
C(28)	9.30	−3.11	0.00	C(27)	C(28)	1.34	C(13)	120.00	C(22)	120.00	Pro-S
O(29)	0.90	−4.65	0.00	O(21)	C(22)	1.36	C(28)	120.00	C(13)	0.00	Dihedral
C(30)	0.90	−3.30	0.00	C(23)	C(22)	1.34	O(21)	120.00	C(28)	120.00	Pro-R
C(31)	−0.26	−2.63	0.00	C(24)	C(23)	1.34	C(22)	120.00	O(21)	180.00	Dihedral
C(32)	−0.26	−1.29	0.00	H(58)	C(23)	1.10	C(22)	120.00	C(24)	120.00	Pro-R
O(33)	−1.43	−0.61	0.00	O(25)	C(24)	1.36	C(23)	120.00	C(22)	180.00	Dihedral
C(34)	0.90	−0.62	0.00	C(26)	C(27)	1.34	C(28)	120.00	C(13)	−180.00	Dihedral
C(35)	2.06	−1.29	0.00	H(60)	C(26)	1.10	C(24)	120.00	C(27)	120.00	Pro-R
C(36)	2.06	−2.63	0.00	H(61)	C(27)	1.10	C(26)	120.00	C(28)	120.00	Pro-S
H(37)	4.08	4.93	0.00	C(15)	C(19)	1.52	C(8)	109.50	C(2)	0.00	Dihedral
H(38)	7.26	6.51	0.00	H(53)	C(19)	1.11	C(8)	109.44	C(15)	109.44	Pro-S
H(39)	10.43	4.93	0.00	H(54)	C(19)	1.11	C(8)	109.46	C(15)	109.46	Pro-R
H(40)	7.26	1.64	0.00	C(16)	C(15)	1.51	C(19)	109.50	C(8)	180.00	Dihedral
H(41)	11.26	−1.47	−0.91	H(49)	C(15)	1.11	C(16)	109.44	C(19)	109.44	Pro-R
H(42)	11.26	−1.47	0.91	H(50)	C(15)	1.11	C(16)	109.46	C(19)	109.46	Pro-S
H(43)	8.85	0.89	0.91	C(18)	C(16)	1.51	C(15)	120.00	C(19)	0.00	Dihedral
H(44)	8.85	0.89	−0.91	O(17)	C(16)	1.21	C(15)	120.00	C(18)	120.00	Pro-S
H(45)	8.78	−1.24	0.91	C(20)	C(18)	1.52	C(16)	109.50	C(15)	−180.00	Dihedral

Because of stretching and bending of the bonds in ARF and RF, cesium, cobalt, and/or europium nitrates solutions labeled with ^{134}Cs, ^{60}Co, and $^{152+154}Eu$ could penetrate the gels through the cavities. The penetration process may be diffusion controlled. However, Lagergren kinetic model was used for studying the rate constant rather than for testing the diffusion process. Lagergren constants are expressed in Table 4 for cesium, cobalt, and/or europium nitrates solutions labeled with ^{134}Cs, ^{60}Co, and $^{152+154}Eu$. The K_{ads}, min^{-1} values deceased with raising the reaction temperatures. In addition, cobalt ion's velocities were intermediate between Eu^{3+} and Cs^{+} ions. By the same way, it found that the K_{ads}, min^{-1} constants inside the ARF is less than in case of RF. This could be attributed to the more flexible structure of ARF rather than RF as could be seen in Tables 2 and 3 [9,10].

Table 5 shows the effect of reaction conditions on both the distribution coefficients and capacities of ARF and RF. Tertiary-butanol, used as a surfactant gave higher capacity and selectivity than span-80 of the prepared ARF gels. However, KOH is less preferred as a catalyst than Na_2CO_3. These results could be attributed to the increased surface area and porosity values, obtained as a result of controlled withdrawal of the t-butanol and decomposition of the remaining Na_2CO_3 to carbon dioxide gas during the

Table 3
Spatial coordinates, Cartesian coordinates, internal coordinates and their corresponding angles of RF gel

Cartesian coordinates				Internal coordinates							
Atom	X (Å)	Y (Å)	Z (Å)	Atom	Bond Atom	Length Ao	Angle atom	Angle (o)	2nd angle atom	2nd angle(o)	
O(1)	3.09	−3.51	0.00	C(2)							
C(2)	4.27	−2.83	0.00	C(3)	C(2)	1.34					
C(3)	4.27	−1.50	0.00	O(1)	C(2)	1.36	C(3)	120.00			
C(4)	5.43	−0.83	0.00	C(8)	C(2)	1.34	O(1)	120.00	C(3)	120.00	Pro-R
O(5)	5.43	0.53	0.00	C(4)	C(3)	1.34	C(2)	120.00	O(1)	180.00	Dihedral
C(6)	6.58	−1.50	0.00	C(9)	C(3)	1.50	C(2)	120.00	C(4)	120.00	Pro-R
C(7)	6.58	−2.83	0.00	O(5)	C(4)	1.36	C(3)	120.00	C(2)	180.00	Dihedral
C(8)	5.43	−3.50	0.00	C(6)	C(4)	1.34	C(3)	120.00	O(5)	120.00	Pro-R
C(9)	2.97	−0.75	0.00	C(7)	C(8)	1.34	C(2)	120.00	O(1)	180.00	Dihedral
C(10)	7.88	−0.75	0.00	C(10)	C(6)	1.50	C(4)	120.00	C(7)	120.00	Pro-R
O(11)	3.23	0.63	0.00	C(20)	C(8)	1.50	C(2)	120.00	C(7)	120.00	Pro-R
O(12)	4.80	−7.69	0.00	H(47)	C(7)	1.10	C(6)	120.00	C(8)	120.00	Pro-R
C(13)	3.77	−6.81	0.00	C(14)	C(20)	1.50	C(8)	109.50	C(2)	0.00	Dihedral
C(14)	4.01	−5.50	0.00	H(57)	C(20)	1.11	C(8)	109.44	C(14)	109.44	Pro-R
C(15)	3.00	−4.63	0.00	H(58)	C(20)	1.11	C(8)	109.46	C(14)	109.46	Pro-S
O(16)	3.25	−3.30	0.00	C(13)	C(14)	1.34	C(20)	120.00	C(8)	180.00	Dihedral
C(17)	1.74	−5.08	0.00	C(15)	C(14)	1.34	C(13)	120.00	C(20)	120.00	Pro-R
C(18)	1.49	−6.39	0.00	O(12)	C(13)	1.36	C(14)	120.00	C(15)	180.00	Dihedral
C(19)	2.51	−7.26	0.00	C(19)	C(13)	1.34	O(12)	120.00	C(14)	120.00	Pro-R
C(20)	5.43	−5.00	0.00	O(16)	C(15)	1.36	C(14)	120.00	C(13)	180.00	Dihedral
C(21)	0.60	−4.10	0.00	C(17)	C(15)	1.34	C(14)	120.00	O(16)	120.00	Pro-R
O(22)	−0.61	−4.80	0.00	C(18)	C(19)	1.34	C(13)	120.00	O(12)	180.00	Dihedral
O(23)	9.16	3.72	0.00	C(21)	C(17)	1.50	C(15)	120.00	C(18)	120.00	Pro-R
C(24)	10.50	3.51	0.00	H(55)	C(18)	1.10	C(17)	120.00	C(19)	120.00	Pro-R
C(25)	11.34	4.54	0.00	H(56)	C(19)	1.10	C(13)	120.00	C(18)	120.00	Pro-R
C(26)	12.66	4.33	0.00	C(35)	C(10)	1.50	C(6)	109.50	C(4)	0.00	Dihedral
O(27)	13.51	5.39	0.00	H(50)	C(10)	1.11	C(6)	109.44	C(35)	109.44	Pro-R
C(28)	13.14	3.09	0.00	H(51)	C(10)	1.11	C(6)	109.46	C(35)	109.46	Pro-S
C(29)	12.30	2.05	0.00	C(36)	C(35)	1.34	C(10)	120.00	C(6)	180.00	Dihedral
C(30)	10.98	2.26	0.00	C(41)	C(35)	1.34	C(10)	120.00	C(36)	120.00	Pro-R
C(31)	10.80	5.94	0.00	C(37)	C(36)	1.34	C(35)	120.00	C(10)	180.00	Dihedral
C(32)	14.62	2.85	0.00	C(42)	C(36)	1.50	C(35)	120.00	C(37)	120.00	Pro-R
O(33)	11.87	6.85	0.00	O(38)	C(37)	1.36	C(36)	120.00	C(35)	180.00	Dihedral
O(34)	14.87	1.47	0.00	C(39)	C(37)	1.34	C(36)	120.00	O(38)	120.00	Pro-R
C(35)	7.61	0.72	0.00	C(40)	C(41)	1.34	C(35)	120.00	C(10)	180.00	Dihedral
C(36)	8.62	1.59	0.00	C(43)	C(39)	1.50	C(37)	120.00	C(40)	120.00	Pro-R
C(37)	8.38	2.91	0.00	H(72)	C(40)	1.10	C(39)	120.00	C(41)	120.00	Pro-R
O(38)	9.41	3.79	0.00	H(73)	C(41)	1.10	C(35)	120.00	C(40)	120.00	Pro-R

drying process, especially at higher temperatures, leading greater porosities of the prepared gels [15,20].

As the conditions are optimized, the capacity and selectivity coefficients of cesium, cobalt, and/or europium nitrate's ions labeled with ^{134}Cs, ^{60}Co, and $^{152+154}Eu$ on ARF and RF resins are in the same order of $Cs^{+} > Co^{2+} > Eu^{3+}$.

This sequence is in accordance with the hydrated radii of the exchanged ions. The ions with smaller hydrated radii easily penetrate the pores of the

Table 4
Lagergren constant k_{ads} (min^{-1}) for various metal ions sorbed on ARF and RF at different reaction temperatures

ARF				RF		
Temperature	Cs^+	Co^{2+}	Eu^{3+}	Cs^+	Co^{2+}	Eu^{3+}
30℃	0.0171	0.0119	0.0163	0.0237	0.0187	0.0245
40℃	0.0133	0.0103	0.0134	0.0219	0.0186	0.0236
50℃	0.0109	0.0086	0.0096	0.0198	0.0173	0.0231
60℃	0.0091	0.0072	0.0055	0.0192	0.0171	0.0197

Table 5
Distribution coefficients and equilibrium capacities of some cations on RF and ARF resins at different conditions

Effect of preparation conditions of ARF on Cs^+ sorption		K_d (mL/g)	Q_e (meq/g)
Effect of Surfactant	t-butanol	380.59	4.98
	Span-80	126.00	3.19
Effect of drying mechanism	Aerogels	2241.83	3.45
	Xerogel	1123.43	5.67
	Cryogels	1260.54	4.63
Effect of catalyst	Na_2CO_3	4900.00	3.94
	KOH	415.70	5.67
ARF/optimized	Cs^+/H^+	9565.70	7.34
	Co^{2+}/H^+	355.18	3.86
	Eu^{3+}/H^+	267.99	2.13
RF/optimized	Cs^+/H^+	1398.53	5.91
	Co^{2+}/H^+	187.63	2.34
	Eu^{3+}/H^+	156.69	2.11

exchanger, resulting in higher adsorption. In addition, the results of ARF possessed higher selectivities and capacities than RF, as explained by the difference to the reaction coordinates and bending of the bonds proved by the FTIR measurements [19,21].

4. Conclusion

ARF and RF were prepared vial sol–gel polycondenstion route and characterized using different schemes. They proved that they have amorphous structures with high surface area and porosity values, which enabled them to be specifically used as sorbent for radioactive cesium as they have good selectivity and capacity orders, compared to other cations. The selectivities and capacities obtained are in accordance with their structural coordinates in space. This would authorize to tailor different ARF and RF gels with controlled properties in the waste-management field.

References

[1] T.A. Vereshchagina, S.N. Vereshchagin, N.N. Shishkina, N.G. Vasilieva, L.A. Solovyov, A.G. Anshits, Microsphere zeolite materials derived from coal fly ash cenospheres as precursors to mineral-like aluminosilicate hosts for ^{135,} 137Cs and ^{90}Sr, J. Nucl. Mater. 437(1–3) (2013) 11–18.
[2] S. Suehara, H. Yamada, Cesium stability in a typical mica structure in dry and wet environments from first-principles, Geochim. Cosmochim. Acta 109(15) (2013) 62–73.
[3] E. Reinoso-Maset, P.J. Worsfold, M.J. Keith-Roach, Effect of organic complexing agents on the interactions of Cs^+, Sr^{2+} and with silica and natural sand, Chemosphere 91(7) (2013) 948–954.
[4] S. Chaudhury, C. Agarwal, A.K. Pandey, A. Goswami, P.U. Sastry, Electrically-driven facilitated transport of Cs^+ across copper ferrocyanide channels in track etched membrane, J. Membr. Sci. 434 (2013) 93–98.
[5] H. Faghihian, H. Iravani, M. Moayed, M. Ghannadi-Maragheh, Preparation of a novel PAN–zeolite nanocomposite for removal of Cs^+ and Sr^{2+} from aqueous solutions: Kinetic, equilibrium, and thermodynamic studies, Chem. Eng. J. 222 (15) (2013) 41–48.
[6] G.M. Ibrahim, B. El-Gammal, I.M. El-Naggar, Selectivity modification of sodium and cesium ions on silicon antimonate, Current Topics Colloid Interf. Sci. 6 (2003) 159.
[7] S.A. Shady, B. El-Gammal, Diffusion pathways of sodium and cesium ions in the particles of titanium(IV) antimonate, Colloids Surf. A: Physicochem. Eng. Aspects 268 (2005) 7–11.
[8] H.H. El-Nahas, F.H. Khalil, G.M. Ibrahim, B. El-Gammal, Preparation of unsaturated polyester-styrene beads using gamma irradiation and chemical polymerization routes for use in the recovery of some alkali metal Ions, J. Appl. Polym. Sci. 104(2) (2007) 1149–1160.
[9] B. El-Gammal, G.M. Ibrahim, K.F. Allan, I.M. El-Naggar, Modeling the PAAc-AN-TV surface using ^{134}Cs and $^{152+154}$Eu sorption, J. Appl. Polym. Sci. 113(5) (2009) 3405–3416.
[10] B. El-Gammal, K.F. Allan, Ion exchange reversibility of some radionuclides on zirconium tungstosuccinate and zirconium tungstosalicylate at their solid-liquid interfaces, Sep. Sci. Technol. 47 (2012) 131–146.
[11] S. S. Metwally, B. El-Gammal, H. F. Aly, S. A. Abo-El-Enein, Removal and separation of some radionuclides by polyacrylamide based Ce(IV) phosphate from radioactive waste solutions, Sep. Sci. Technol.46 (2011) 1808–1821.
[12] B. El-Gammal, S.S. Metwally, H.F. Aly, S.A. Abo-El-Enein, Verification of double-shell model for sorption of cesium, cobalt, and europium ions on polyacrylonitrile-based Ce(IV) phosphate from aqueous solutions, Desalin. Water Treat. 46 (2012) 1–15.
[13] N.M. Hassan, K. Adu-Wusu, J.C. Marra, Resorcinol-formaldehyde adsorption of cesium from Hanford waste solutions, Part I. Batch equilibrium study, J. Radioanal. Nucl. Chem. 262(3) (2004) 579–586.
[14] N. Tonanon, W. Intarapanya, W. Tanthapanichakoon, H. Nishihara, S. R. Mukai, H. Tamon, Submicron mesoporous carbon spheres by ultrasonic emulsification, J. Porous Mater. 15 (2008) 265–270.
[15] D. Fujikawa, M. Uota, G. Sakai, T. Kijima, Shape-controlled synthesis of nanocarbons fromresorcinol–formaldehyde resorcinol–formaldehyde nanopolymers using surfactant-templated vesicular assemblies, Carbon 45 (2007) 1289–1295.
[16] K. Nakamoto, Infrared and Raman Spectra of Inorganic and Coordination Compounds, 6th ed., John Wiley and Sons, Hoboken, NJ, 2009.
[17] C. Dwivedi, A. Kumar, J.K. Ajish, K. Kant Singh, M. Kumar, P. Kishen Wattalb, P. N. Bajaja, Resorcinol-formaldehyde coated XAD resin beads for removal of cesium ions from radioactive waste: Synthesis, sorption and kinetic studies, RSC Advances 2 (2012) 5557–5564.

[18] G.M. Ibrahim, M.I. Ahmad, B. El-Gammal, Structural development Of TMMA and SSQXN-8 as porous chelating resins, J. Appl. Polym. Sci. 113(5) (2009) 3038–3048.
[19] S.A. Shady, Selectivity of cesium from fission radionuclides using resorcinol–formaldehyde and zirconyl-molybdopyrophosphate as ion-exchangers, J. Hazard. Mater. 167 (2009) 947–952.
[20] T. Yamamoto, T. Nishimura, T. Suzuki, H. Tamon, Effect of drying method on mesoporosityof resorcinol-formaldehyde dry gel and carbon gel, J. Drying Technol. 19(7) (2001) 1319–1333.
[21] D. Ding, Y. Zhao, S. Yang, W. Shi, Z. Zhang, Z. Lei, Y. Yang, Adsorption of cesium from aqueous solution using agricultural residue—Walnut shell: Equilibrium, kinetic and thermodynamic modeling studies, Water Res. 47(7) (2013) 2563–2571.